

Preparation and characterization of the shape-stabilized phase change material based on sebacic acid and mesoporous MCM-41

Lipeng Han^{1,2} · Guixiang Ma^{1,2} · Shaolei Xie¹ · Jinhe Sun¹ · Yongzhong Jia¹ · Yan Jing¹

Received: 10 August 2016 / Accepted: 9 May 2017 / Published online: 26 May 2017
© Akadémiai Kiadó, Budapest, Hungary 2017

Abstract Shape-stabilized composite phase change materials composed of sebacic acid (SA) and MCM-41 were prepared by a facile blending and impregnating method. Various characterization techniques were carried out to characterize their structural and thermal properties, including thermogravimetry (TG) analyses and differential scanning calorimetry (DSC), X-ray diffraction (XRD), Fourier transform infrared spectroscopy (FT-IR), and scanning electron microscopy. The XRD and FT-IR results indicated the interactions between SA and MCM-41, such as the capillary force and the hydrogen bonding, resulting in the confined crystallization process. As a result, the SA that was confined was amorphous. The TG analysis results showed that the presence of MCM-41 practically resulted in an overlapping of the two decomposition stages. The DSC analysis demonstrated that a decrease in the SA content was accompanied by a continuous decrease in the melting point and phase change enthalpy of the composites.

Keywords Phase change materials · Thermal properties · Sebacic acid · MCM-41

Introduction

Efficient energy storage devices and systems can improve energy efficiency to reduce the gap between supply and demand of energy. Of the many options considered, phase change materials (PCMs) have attracted great interest in the scientific and industry community [1–3]. In recent years, PCMs have become a hotspot in the fields of solar heating system, building energy conservation, air-conditioning systems, thermal insulation and regulation, waste heat recovery, and so on, due to their high energy storage density, isothermal operating characteristics, and extremely small temperature variation [4–7].

Among various PCMs, organic PCMs are of great importance in thermal energy storage. Well-known organic PCMs include linear chain hydrocarbons (paraffins), polyethylene glycols, fatty acids, carboxylic acids, and organic eutectic mixtures. Compared with inorganic PCMs, organic PCMs have numerous advantages, such as chemically stable, free from supercooling, non-phase segregation [8, 9].

Among various organic PCMs, sebacic acid (SA) is a dicarboxylic acid, possessing a melting point of 133.3 °C and latent heat over 222.4 J g⁻¹ [10, 11]. SA is considered to be a promising PCM owing to its suitable phase change temperature, high latent heat capacity, congruent melting, and lack of supercooling. However, there are three problems: (1) leakage from the thermal storage system when the SA is heated to melt, (2) volume changes in the PCM during phase change, and (3) relatively strong corrosivity. These obstacles result in lower thermal efficiency and constrain applications of SA [12, 13].

Some researchers have demonstrated that using porous materials as containers for PCMs can avoid the liquid leakage and corrosion behavior of energy storage units.

✉ Jinhe Sun
jinhesun@163.com

✉ Yongzhong Jia
jiayzh@hotmail.com

¹ Key Laboratory of Comprehensive and Highly Efficient Utilization of Salt Lake Resources, Qinghai Institute of Salt Lakes, Chinese Academy of Sciences, Xining 810008, China

² University of Chinese Academy of Sciences, Beijing 100049, China

Kadoono et al. [14] prepared the composites of siliceous SBA-15 or carbonaceous CMK-3 mesoporous assemblies and stearic acid, which could be used to make leak-free devices that retain their capabilities over many thermal cycles. Abu-Zied et al. synthesized MCM-41/polyethylene glycol composites and found that Si–OH groups of MCM-41 reacted with the OH groups in PEG. This reaction resulted in more restricted PEG segments in the MCM-41/PEG composites, which, in turn, prevented the leakage of the melted PEG from the stabilizer. In addition, thermogravimetry (TG) results indicated that the thermal oxidative degradation of PEG, in the presence of MCM-41, started earlier than neat PEG. In other word, MCM-41/PEG composites presented lower thermal stability [15]. Zhang et al. [16] studied the structure and thermal performance of poly(ethylene glycol) alkyl ether (Brij)/porous silica (MCM-41) composites as shape-stabilized PCMs. Feng et al. [17] studied shape-stabilized PCMs composed of polyethylene glycol and various mesoporous matrices (AC, SBA-15, and MCM-41) to avoid leakage of the liquid phase that occurs above the phase change point.

In addition, other matrixes have been widely reported, including polymers, silica, diatomite, bentonite, vermiculite, perlite, attapulgite, montmorillonite, expanded graphite, and metal foam [18–25]. Among these matrixes, mesoporous silica materials have become the focus of a great deal of recent research in the field of nanostructured materials because of their periodic structure, uniform pores, and extremely high surface areas, which are excellent hosts for other materials to avoid leakage of PCMs [26–28].

Other characteristics of mesoporous silica materials, such as excellent chemical stability, good thermal conductivity, high mechanical strength, and fire resistance, are also attractive characteristics to enhance their thermal performances.

In this study, SA/MCM-41 PCMs composed of SA components and porous materials (MCM-41) were fabricated through the physical mixing method. Various characterization methods such as Fourier transform infrared spectroscopy (FT-IR), X-ray diffraction (XRD), differential scanning calorimetry (DSC), scanning electron microscopy (SEM), and TG analysis were utilized to characterize and verify the properties of the obtained composites.

Experimental

Materials

In this investigation, sebacic acid (SA) with a purity of 99% was purchased from Shanghai Aladdin Industrial Co.

Ltd. Porous MCM-41 was obtained from Nanjing XFNANO Materials Tech Co. Ltd., the average pore diameter is 3.4 nm, and the specific surface area is above $850 \text{ m}^2 \text{ g}^{-1}$. Ethanol (purity 99.7%) was purchased from Tianjin Yongda Chemical Reagent Technology Co. Ltd.

Preparation of the shape-stabilized PCMs

Shape-stabilized PCMs were prepared using the direct blending and impregnating operation in air. The MCM-41 and SA with different mass percentages (90, 80, 70, 60, and 50%) were mixed in a round-bottom flask. Absolute ethanol was added, and the solution was then stirred vigorously by using thermostat oil bath with magnetic stirring function (HH-ZKYY, Shanghai Hujia Instrument Equipment Co. Ltd.) for 2 h. After this, the mixture was dried in vacuum drying oven (VH, Nanjing Jiaodian Machinery Equipment Co., Ltd.) at $80 \text{ }^\circ\text{C}$ until the ethanol evaporated.

Characterization

Thermal properties of the composite PCMs, such as melting point and latent heat, were measured using a Mettler Toledo DSC2. The measurements were performed at 2 or 10 K min^{-1} in heating and cooling procedure in nitrogen atmosphere. The temperature accuracy was $\pm 0.01 \text{ }^\circ\text{C}$, and the heat flow repeatability was $0.2 \text{ } \mu\text{W}$. Powder X-ray diffractograms were recorded from 5° to 70° with a step of 1° s^{-1} using a PANalytical (X'pert BRO, Holland) instrument with a Ni-filtered Cu $\text{K}\alpha$ radiation source ($\lambda = 0.15418 \text{ nm}$) operated at 40 kV and 30 mA. FT-IR spectra were recorded using a Thermo Nicolet NEXUS FT-IR spectrometer. A resolution of 4 cm^{-1} and the average of 32 automated scans from 400 to 4000 cm^{-1} were used to obtain the FT-IR spectra. TG curves were recorded using a Netzsch instruments (STA 449F3) TG analyzer at a scan rate of 5 K min^{-1} under an atmosphere of nitrogen. The SEM morphology of the samples was analyzed by a JEOL model JSM-5610LV microscope.

Results and discussion

Chemical properties of SA and the composite PCMs

Figure 1 shows the FT-IR spectrum of pure SA, mesoporous materials, and the composite PCMs. In the FT-IR spectrum of SA, the peak at 1698 cm^{-1} represents the stretching vibration of the C=O group. The peaks at 2934 and 2852 cm^{-1} signify the stretching vibration of the single $-\text{CH}_2$ group. The peak at 1430 cm^{-1} is assigned to the bending vibration of the single $-\text{CH}_2$ group. The peak at 721 cm^{-1} represents the swinging vibration of the

$-\text{CH}_2$ group, a feature of $(\text{CH}_2)_8$ [10]. On the spectra of the silica stabilizers (MCM-41), peaks at 3440 and 1641 cm^{-1} are assigned to the stretching vibration of hydroxyl and water, respectively. The peaks at 1082 , 801 , and 464 cm^{-1} represent the bending vibration of the Si–O functional group [17].

After comparing the spectra of the composite PCMs with those of the mesoporous stabilizer and pure SA, these adsorption peaks could also be observed in the spectra of the composite PCMs and no obvious new peaks were observed. However, some absorption peaks of the composites had a slight shift. The FT-IR results suggested that there were C=O and O–H groups in both SA and MCM-41. Therefore, the hydrogen bonds inferred from the frequency shifts of the functional group also existed between SA and the porous materials.

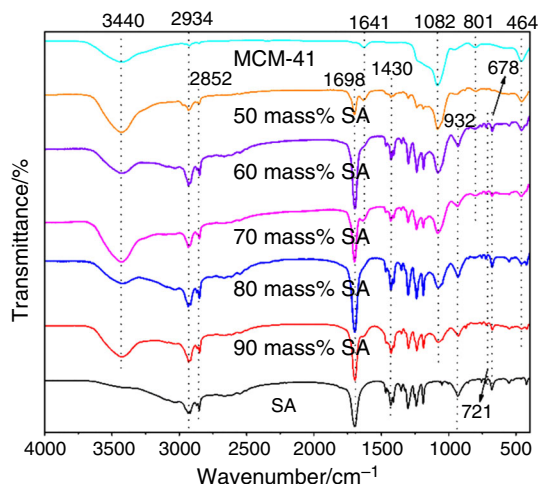
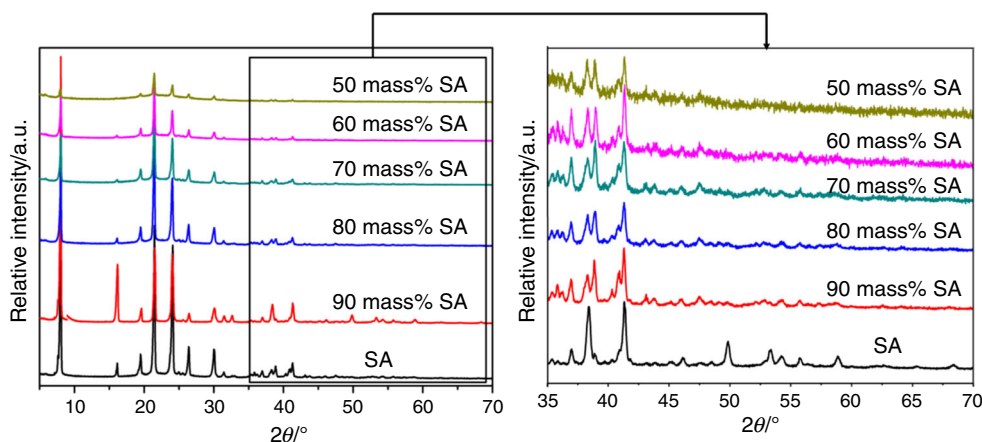


Fig. 1 FT-IR spectrum of pure SA, MCM-41 and the composite PCMs. These featured band characteristics of SA and MCM-41 indicated as the dot line in the figure

Fig. 2 Wide-angle XRD diffractograms obtained for pure SA and composites with MCM-41



Crystallization properties of SA and the composite PCMs

It is well known that the crystal structure and the crystallization behavior of molecules altered when the organic or inorganic nucleated agents were used. And, when molecular chains are confined or absorbed by some porous materials, the crystallization behavior will exhibit the different crystallization process, i.e., confined crystallization and nucleation-induced crystallization [16].

Figure 2 shows the wide-angle XRD patterns of pure SA and the composite PCMs. From Fig. 2, the 2θ position of the peaks for the composite PCMs was basically the same as that of pure SA, meaning that introducing the mesoporous stabilizer did not affect the crystal structure of SA. However, it's worth noting that the crystallinity and relative diffraction intensity of the confined phase of SA were totally different than those of the bulk crystal, which demonstrated that the porous structure of MCM-41 affected the crystalline behavior of SA molecules. This might be due to the contribution of interactions with MCM-41, such as the capillary force and the hydrogen bonding, resulting in the confined crystallization process. As a result, the SA that was confined was amorphous. Similarly, Feng et al. [17] and Jiang et al. [29] also observed the confined crystallization behavior in their studies.

Micromorphology analysis

Figure 3a presents the surface of the pure MCM-41 material. It showed that accumulative spherical particles had an average diameter of $100\text{--}1000 \text{ nm}$. Moreover, it could be found that there was some shapeless space between discrete particles. As illustrated in Fig. 3b–f, these composited PCMs constituted the obvious interpenetrate networks, which could well accommodate SA into the porous MCM-41 materials. A homogeneous and

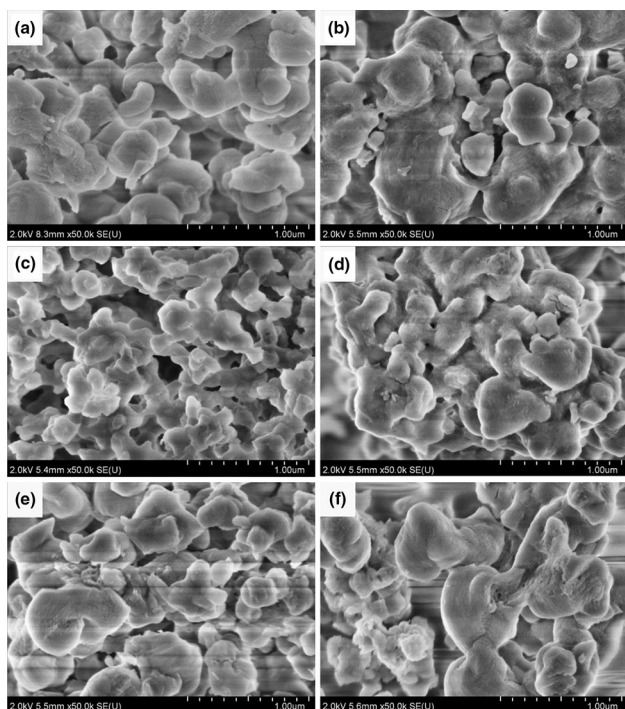


Fig. 3 SEM images of MCM-41 and the composites **a** MCM-41, **b** 50 mass% SA, **c** 60 mass% SA, **d** 70 mass% SA, **e** 80 mass% SA, **f** 90 mass% SA

smooth morphology could be perceived easily with increasing mass percentage of SA. Meanwhile, the unfavorable voids between particles were getting smaller. In other words, SA molecules could not only crystallize onto the MCM-41 surface but also in the inner pore of MCM-41 networks. This uniform encapsulation also indicated good cohesion between the inorganic particles and SA, which was due to the effect of capillary and surface tension force.

Thermal behavior of SA/MCM-41 composited PCMs

The phase change temperature and latent heat of composites were measured with the DSC technique. Figure 4a, b demonstrates the heating and cooling DSC curves of pure SA and composites with various SA mass fractions at a heating and cooling rate of 10 K min^{-1} . The corresponding phase change parameters obtained from the DSC evaluation are summarized in Table 1. It could be seen that SA showed the obvious phase change process, and the onset melting (T_{m0}) and crystallizing (T_{c0}) temperature appeared at 131.7 and 129.8 °C, respectively. The phase change enthalpy ΔH_m of SA was 222.3 J g^{-1} . However, a gradual continuous decrease in the melting point with increasing MCM-41 can be observed.

Fig. 4 DSC curves of SA and SA/MCM-41 composited PCMs with the different amount of SA components **a** heating process at a rate of 10 K min^{-1} , **b** cooling process at a rate of 10 K min^{-1} , **c** heating process at a rate of 2 K min^{-1} , **d** cooling process at a rate of 2 K min^{-1}

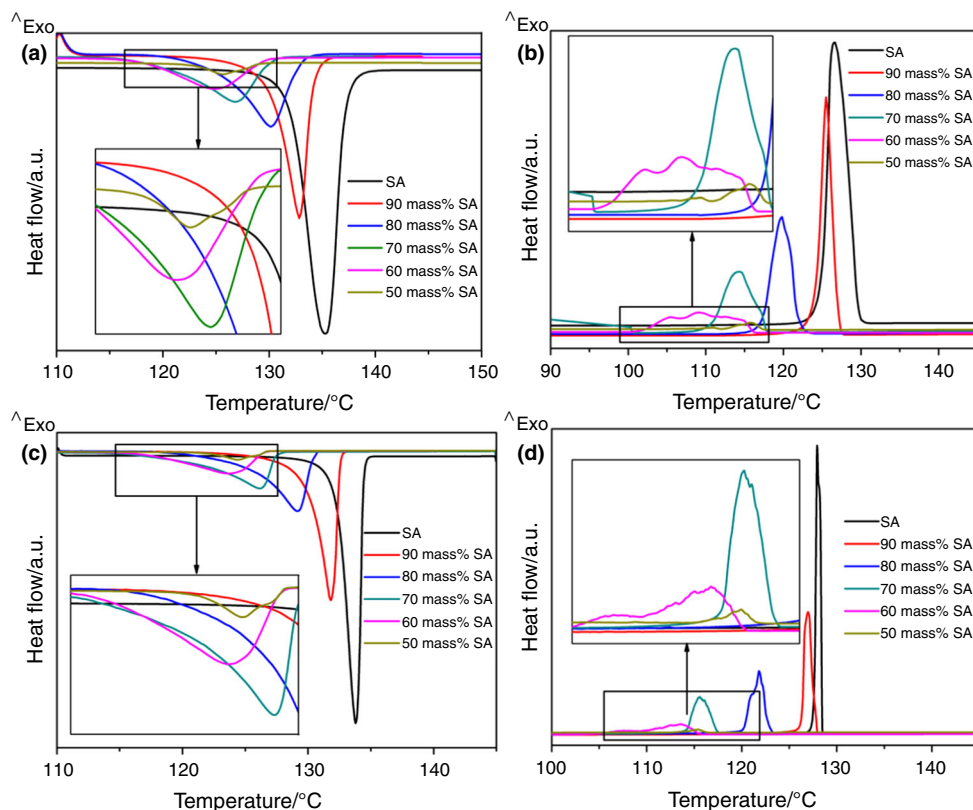
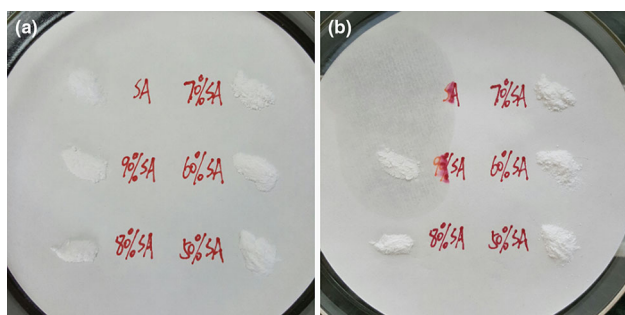


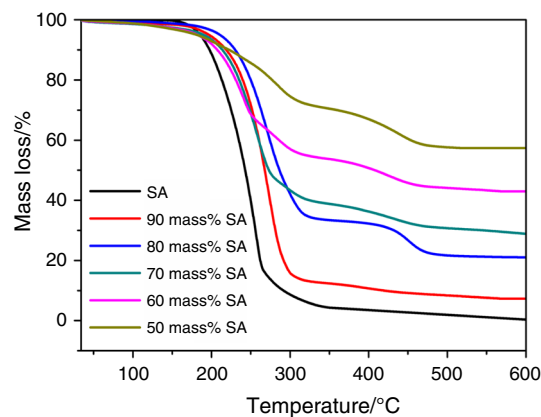
Table 1 Thermographic data of SA and SA/MCM-41 composited PCMs

Samples	10 K min ⁻¹				2 K min ⁻¹			
	$\Delta H_m/J\ g^{-1}$	$T_{mo}/^{\circ}C$	$\Delta H_c/J\ g^{-1}$	$T_{co}/^{\circ}C$	$\Delta H_m/J\ g^{-1}$	$T_{mo}/^{\circ}C$	$\Delta H_c/J\ g^{-1}$	$T_{co}/^{\circ}C$
Pure SA	222.3	131.7	222.1	129.8	132.3	221.8	219.2	129.9
SA (90 mass%)/MCM-41	186.6	129.8	185.1	127.2	183.7	130.0	183.2	127.8
SA (80 mass%)/MCM-41	125.1	125.1	124.6	122.1	125.9	125.4	125.7	122.8
SA (70 mass%)/MCM-41	89.4	120.1	88.6	118.0	89.3	121.0	88.8	117.4
SA (60 mass%)/MCM-41	63.6	118.0	62.1	116.2	64.8	117.3	59.4	115.3
SA (50 mass%)/MCM-41	14.4	122.6	13.9	117.4	14.8	121.9	14.1	116.3

**Fig. 5** Photograph of SA and composited PCMs with different mass percentage of SA **a** before heating process, **b** treated at 150 °C for 1 h

Perhaps fast heating and cooling rates of 10 K min⁻¹ made the SA of the composites in the inner pore of MCM-41 networks failed to fully melt and crystallize. Hence, extra measurements were then completed at a lower heating and cooling rate of 2 K min⁻¹. Figure 4c, d shows that the thermal behavior of composited PCMs at the heating and cooling rates of 2 K min⁻¹ was very close to the former measurements. The speed of heating and cooling did not affect the thermal behavior of the composites.

These changes in the phase change temperatures of composited PCMs were most likely due to the interactions characterized by FT-IR [30]. In consideration of decrease in the latent heat of the composite PCMs, lower fraction of SA could not be the only reason. Another factor was that the blending of mesoporous matrices interfered with the crystallization of SA. Some SA molecule chains were in the confined condition and could not be crystallized freely. Thus, increasing amorphous SA resulted in the smaller enthalpy. So, in combination with DSC results and XRD results, it indicated that two possible crystallization processes, i.e., the nucleation-induced crystallization and the confined crystallization behavior, existed in SA/MCM-41 PCMs. Therefore, these results also demonstrated that the changes of confined environments have the important effect on the crystalline structure and stacking manners of molecular chains [31, 32].

**Fig. 6** TG curves of pure SA and composited PCMs with different amount of SA components in MCM-41 materials

Thermal stability

The shape stability of PCMs is one important standard to evaluate their perspective in future applications. To detect the leakage behavior of these composites, the composites were placed onto the filter paper and then put them into the oven at 150 °C for 1 h. Digital photographs of bulk SA and SA/MCM-41 composited PCMs after the heating and cooling process are shown in Fig. 5.

From the compared results, it could be clearly found that pure SA and composite with 90 mass% SA showed the molten and flow state once when the temperature was above its melting point. A few leakage spots on the filter paper could be still found in the composite with 80 mass% SA. And there was no leakage of the liquid phase when the mass percentage of SA in the composites was lower than 80 mass%. It indicated that the interactions between SA and porous materials and the capillary force between the SA and the pores could provide composited PCMs with the good structure stable properties when the mass percentage of MCM-41 was higher than 20 mass%.

The SA and the various SA/MCM-41 composites were then verified using TG analyses in order to further understand the thermal stability of them. Figure 6 shows TG

curves of pure SA and the composite PCMs. It could be seen that pure SA and composite with 90 mass% SA showed one-step decomposition process. In addition, an overlapping of the two stages became apparent as the content of MCM-41 increased. According to Fig. 6, it is obvious that the last decomposition step of SA/MCM-41 composites was very slow, which occurred through a wide range of temperatures ($>100\text{ }^{\circ}\text{C}$). Such stages were most likely related to the fraction of SA inside the channels and to the fraction that surrounded the filler particles [33].

Conclusions

In this paper, the shape-stabilized composited PCMs composed of MCM-41 as the supporting materials and SA with the mass percentage ranging from 50 to 90 mass% as the PCM were prepared by the direct blending and impregnating method. When the composites ($\omega_{\text{SA}} > 70\text{ mass}\%$) were heated to melt, it could be found that there was some leakage of the liquid phase. According to the FT-IR and XRD results, interactions between SA and MCM-41, such as the capillary force and the hydrogen bonding, resulted in the confined crystallization process. As a result, the SA that was confined was amorphous. DSC data of SA/MCM-41 composites showed that there was a continuous decrease in the SA melting point and phase change enthalpy with increasing MCM-41. As compared to pure SA, the melting point was reduced from 131.7 to 118.0 $^{\circ}\text{C}$ at 60 mass% SA loading. This observed decrease in melting point and phase change enthalpy, in turn, provided insight into the FT-IR and XRD results. TG curves demonstrated that an overlapping of the two stages became apparent with increasing MCM-41. Thermal stabilities of the SA/MCM-41 composites have been strengthened. Taking into account the properties of the largest latent heat, relatively low melting point, the minimal leakage, composite with 70 mass% SA is the most promising candidate for heat storage application.

Acknowledgements The authors are pleased to acknowledge financial support from the National Natural Science Foundation of China (No. U1407205) for this research project.

References

1. Yu H, Gao J, Chen Y, Zhao Y. Preparation and properties of stearic acid/expanded graphite composite phase change material for low-temperature solar thermal application. *J Therm Anal Calorim.* 2016;124:87–92.
2. Farid MM, Khudhair AM, Razack SAK, Al-Hallaj S. A review on phase change energy storage: materials and applications. *Energy Conv Manag.* 2004;45:1597–615.
3. Dutil Y, Rousse DR, Salah NB, Lassue S, Zalewski L. A review on phase-change materials: mathematical modeling and simulations. *Renew Sust Energy Rev.* 2011;15:112–30.
4. Duan ZJ, Zhang HZ, Sun LX, Cao Z, Xu F, Zou YJ, Zhou HY. $\text{CaCl}_2 \cdot 6\text{H}_2\text{O}$ /expanded graphite composite as form-stable phase change materials for thermal energy storage. *J Therm Anal Calorim.* 2014;115:111–7.
5. Li W, Song G, Li S, Yao Y, Tang G. Preparation and characterization of novel MicroPCMs (microencapsulated phase-change materials) with hybrid shells via the polymerization of two alkoxy silanes. *Energy.* 2014;70:298–306.
6. Zhong L, Zhang X, Luan Y, Wang G, Feng Y, Feng D. Preparation and thermal properties of porous heterogeneous composite phase change materials based on molten salts/expanded graphite. *Sol Energy.* 2014;107:63–73.
7. Qian T, Li J, Min X, Deng Y, Guan W, Ma H. Polyethylene glycol/mesoporous calcium silicate shape-stabilized composite phase change material: preparation, characterization, and adjustable thermal property. *Energy.* 2015;82:333–40.
8. Memon SA. Phase change materials integrated in building walls: a state of the art review. *Renew Sust Energy Rev.* 2014;31:870–906.
9. Anisur MR, Mahfuz MH, Kibria MA, Saidur R, Metselaar IHSC, Mahlia TMI. Curbing global warming with phase change materials for energy storage. *Renew Sust Energy Rev.* 2013;18:23–30.
10. Wang S, Qin P, Fang X, Zhang Z, Wang S, Liu X. A novel sebacic acid/expanded graphite composite phase change material for solar thermal medium-temperature applications. *Sol Energy.* 2014;99:283–90.
11. Seki Y, Ince S, Ezan MA, Turgut A, Ereğ A. Graphite nanoplates loading into eutectic mixture of Adipic acid and Sebacic acid as phase change material. *Sol Energy Mater Sol Cells.* 2015;140:457–63.
12. Karaipekli A, Bicer A, Sarı A, Tyagi VV. Thermal characteristics of expanded perlite/paraffin composite phase change material with enhanced thermal conductivity using carbon nanotubes. *Energy Conv Manag.* 2017;134:373–81.
13. Wang C, Feng L, Li W, Zheng J, Tian W, Li X. Shape-stabilized phase change materials based on polyethylene glycol/porous carbon composite: the influence of the pore structure of the carbon materials. *Sol Energy Mater Sol Cells.* 2012;105:21–6.
14. Kadoono T, Ogura M. Heat storage properties of organic phase-change materials confined in the nanopore of mesoporous SBA-15 and CMK-3. *Phys Chem Chem Phys.* 2014;16:5495–8.
15. Abu-Zied BM, Hussein MA, Asiri AM. Development and characterization of the composites based on mesoporous MCM-41 and polyethylene glycol and their properties. *Compos Eng.* 2014;58:185–92.
16. Zhang L, Shi H, Li W, Han X, Zhang X. Structure and thermal performance of poly(ethylene glycol) alkyl ether (Brij)/porous silica (MCM-41) composites as shape-stabilized phase change materials. *Thermochim Acta.* 2013;570:1–7.
17. Feng L, Zhao W, Zheng J, Frisco S, Song P, Li X. The shape-stabilized phase change materials composed of polyethylene glycol and various mesoporous matrices (AC, SBA-15 and MCM-41). *Sol Energy Mater Sol Cells.* 2011;95:3550–6.
18. Alkan C, Sari A. Fatty acid/poly(methyl methacrylate)(PMMA) blends as form-stable phase change materials for latent heat thermal energy storage. *Sol Energy.* 2008;82:118–24.
19. Fang Y, Kang H, Wang W, Liu H, Gao X. Study on polyethylene glycol/epoxy resin composite as a form-stable phase change material. *Energy Conv Manag.* 2010;51:2757–61.
20. Qian T, Li J, Ma H, Yang J. Adjustable thermal property of polyethylene glycol/diatomite shape-stabilized composite phase change material. *Polym Compos.* 2016;37:854–60.
21. Qian TT, Li JH, Ma HW, Yang J. The preparation of a green shape-stabilized composite phase change material of polyethylene glycol/SiO₂ with enhanced thermal performance based on oil shale ash via temperature assisted sol-gel method. *Sol Energy Mater Sol Cells.* 2015;132:29–39.

22. Pielichowska K, Pielichowski K. Phase change materials for thermal energy storage. *Prog Mater Sci.* 2014;65:67–123.
23. Wang Y, Wang SY, Wang JP, Yang R. Preparation, stability and mechanical property of shape-stabilized phase change materials. *Energy Build.* 2014;77:11–6.
24. Xiao X, Zhang P, Li M. Preparation and thermal characterization of paraffin/metal foam composite phase change material. *Appl Energy.* 2013;113:1357–66.
25. Li W, Zhang R, Jiang N, Tang XF, Shi HF, Zhang XX, et al. Composite macrocapsule of phase change materials/expanded graphite for thermal energy storage. *Energy.* 2014;57:607–14.
26. Sugino K, Oya N, Yoshie N, Ogura M. A simple modification creates a great difference: new solid-base catalyst using methylated N-substituted SBA-15. *J Am Chem Soc.* 2011;133:20030–2.
27. Costa MJ, Chellappa T, Araujo AS, Fonseca VM, Fernandes VJ, Nascimento RM, Pacheco JG. Characterization and acidic properties of AlMCM-41 prepared by conventional and post-synthesis aluminations. *Aust J Chem.* 2015;68:99–105.
28. Li Q, Li Z, Yu H, Pan X, Wang X, Wang Y, Song J. Effects of ordered mesoporous silica on the performances of composite nanofiltration membrane. *Desalination.* 2013;327:24–31.
29. Jiang S, Yu D, Ji X, An L, Jiang B. Confined crystallization behavior of PEO in silica networks. *Polymer.* 2000;41:2041–6.
30. Karaman S, Karaipekli A, Sari A, Bicer A. Polyethylene glycol (PEG)/diatomite composite as a novel form-stable phase change material for thermal energy storage. *Sol Energy Mater Sol Cells.* 2011;95:1647–53.
31. Wang BH, Xi HA, Yin J, Qian XF, Zhu ZK. Molecular orbital confinement effect of mesoporous silica of MCM-41 on conjugated polymer. *Synth Met.* 2003;139:187–90.
32. Huang P, Zhu L, Cheng SZ, Ge Q, Quirk RP, Thomas EL, Yeh F. Crystal orientation changes in two-dimensionally confined nanocylinders in a poly(ethylene oxide)-b-polystyrene/polystyrene blend. *Macromolecules.* 2001;34:6649–57.
33. Cerrada ML, Pérez E, Lourenço JP, Campos JM, Ribeiro MR. Hybrid HDPE/MCM-41 nanocomposites: crystalline structure and viscoelastic behaviour. *Microporous Mesoporous Mater.* 2010;130:215–23.